Sensors and Actuators B 195 (2014) 549–561

Contents lists available at ScienceDirect

Sensors and Actuators B: Chemical

journal homepage: www.elsevier.com/locate/snb

Self-assembled and Pd decorated Zn_2SnO_4/ZnO wire-sheet shape nano-heterostructures networks hydrogen gas sensors

Bing Wang [a,b,*], Zhao Qiang Zheng [a], Lian Feng Zhu [c], Yu Hua Yang [d], Huan Yu Wu [a]

[a] Shenzhen Key Lab of Micro-nano Photonic Information Technology, College of Electronic Science and Technology, Shenzhen University, Shenzhen 518060, Guangdong, PR China
[b] Shenzhen Key Laboratory of Sensor Technology, Shenzhen University, Shenzhen 518060, PR China
[c] Department of Materials Science and Engineering, Tsinghua University, Beijing 100084, PR China
[d] State Key Laboratory of Optoelectronic Materials and Technologies, Nanotechnology Research Center, School of Physics & Engineering, Sun Yat-sen University, Guangzhou 510275, Guangdong, PR China

ARTICLE INFO

Article history:
Received 6 August 2013
Received in revised form 14 January 2014
Accepted 20 January 2014
Available online 30 January 2014

Keywords:
Gas sensor
Nano-heterostructures
Zn_2SnO_4
ZnO
Self-assembled
Hydrogen sensor

ABSTRACT

Zn_2SnO_4/ZnO wire-sheet shape hetero-nanostructures (Zn_2SnO_4/ZnO HNS) networks gas sensors have been fabricated on Cr comb-shaped interdigitating electrodes with relatively narrower interspace of 1.5 μm using thermal evaporation of the mixed powders of ZnO, SnO_2 and active carbon with Au catalysts. The self-assembly grown sensors of Zn_2SnO_4/ZnO HNS networks have excellent gas sensing characteristics to hydrogen concentration ranging from 2 to 1000 ppm at operating temperature of 120–300 °C. Comparing with Zn_2SnO_4/ZnO HNS networks sensors, the Pd decorated Zn_2SnO_4/ZnO HNS (Pd-Zn_2SnO_4/ZnO HNS) networks sensors exhibit enhanced hydrogen sensing performance such as higher response (74% at 255 °C to 1000 ppm H_2), less response time (15 s at 270 °C to 1000 ppm H_2), better selectivity (response to H_2, C_2H_5OH, CH_4, C_2H_2, CO, and C_3H_8), lower adsorption activation energy (12.72 kJ/mol to 1000 ppm H_2) and smaller deviation from the ideal value of power exponent β (0.49623 at 255 °C). The enhanced sensing properties of the Pd-Zn_2SnO_4/ZnO HNS can be ascribed to an additional depletion layer at the interface between Pd nanoparticles and Zn_2SnO_4/ZnO HNS. Both sensors show fine long-term stability during exposure to 2–1000 ppm H_2 under relatively high operating temperature of 120–300 °C in 50 days.

1. Introduction

1D nano-heterostructures consisting of different materials may combine the different physical or chemical properties into one structure. Moreover, due to the formation of the heterojunction between different materials with various band gaps, the nano-heterostructures are expected to possess some novel electric and optical properties [1]. Recently, significant progress has been made in regard to synthesis of various axial, radial and branched 1D nano-heterostructure. However, reports on the synthesis of 1D nano-heterostructures composited with two kinds of direct wide-band-gap semiconductor of Zn_2SnO_4 with a band gap of about 3.6 eV and ZnO with a large exciton binding energy of 60 meV are very limited [2,3]. In this contribution, we report that a new Zn_2SnO_4/ZnO wire-sheet shape hetero-nanostructures (Zn_2SnO_4/ZnO HNS) have been synthesized via thermal evaporation and condensation with Au catalysts.

The ZnO nanostructures have been considered as ideal building blocks for high responsive gas sensor to detect O_2, H_2, C_2H_5OH, CO, and so on [4–7]. In addition, Zn_2SnO_4 has also been studied for the applications as gas sensors to detect i-C_4H_{10}, NO_2, C_2H_5OH, CO and H_2 [8–12]. Considering scarce of reports being about gas sensing properties of Zn_2SnO_4/ZnO HNS, we report the self-assembly of good selective, highly sensitive and fast responsive H_2 sensors of Zn_2SnO_4/ZnO HNS networks on Cr comb-shape interdigitating electrodes with relatively narrower interspace of 1.5 μm for the hydrogen concentration ranging from 2 to 1000 ppm.

For metal-oxide semiconductor nanostructures, the activity of gas sensing performance is usually promoted by means of decoration with catalytic noble metals such as Pd [13–15], Pt [16], Au [17], etc. Besides, Pd has been commonly used as H_2 sensing material with high response and selectivity because of its high H_2 solubility [15]. Hence, decorating Zn_2SnO_4/ZnO HNS networks with Pd nanoparticles is expected to harvest a high-performance H_2 gas

* Corresponding author at: Shenzhen Key Lab of Micro-nano Photonic Information Technology, College of Electronic Science and Technology, Shenzhen University, Shenzhen, 518060, Guangdong, PR China. Tel.: +86 755 2655 8252; fax: +86 755 2653 4624.
E-mail address: wangbing@szu.edu.cn (B. Wang).

0925-4005/
http://dx.doi.org/10.1016/j.snb.2014.01.073

sensor. However, the corresponding reports have been scarce up to now. In this contribution, we report that Zn_2SnO_4/ZnO HNS decorated with Pd nanoparticles (Pd-Zn_2SnO_4/ZnO HNS) networks sensors have enhanced H_2 sensing performance comparing with the Zn_2SnO_4/ZnO HNS networks sensors.

2. Experimental details

The self-assembly of Zn_2SnO_4/ZnO HNS hydrogen sensors includes two parts. One is the preparation of comb-shape interdigitating electrodes with relatively narrower interspace of 1.5 μm on the Si substrate as shown in Fig. 1a, and the corresponding processes are basically same with our previous works [18].

Another part is the fabrication of Zn_2SnO_4/ZnO HNS on the Si substrate with the comb-shaped interdigitating electrodes by themetallic catalyst-assisted thermal evaporation of active carbon, ZnO and SnO_2 powders. The Au layer (about 5 nm in thickness) is deposited on Si substrate with the electrodes by sputtering. The active carbon, ZnO and SnO_2 powders are mixed in a 3:2:1 weight ratio as the reaction source and put near the Si substrate with the electrodes, which are placed inside the little quartz tube that is pulled into a large quartz tube in a horizontal tube electric furnace. After the whole system evacuated by a vacuum pump for 20 min, the N_2 gas is guided into the system at 50 sccm and the pressure is kept at 300 Torr. Then, the system is rapidly heated up to 800 °C from the room temperature and kept this temperature for 10 min. Finally, the system is cooled down to the room temperature in several hours. The Zn_2SnO_4/ZnO HNS gas sensor chip shown in Fig. 1b is fabricated. Field-emission scanning electron microscopy (FE-SEM, Hitachi/SU-70) and high-resolution transmission electron microscopy (HR-TEM, Jeol/JEM-2010) are used to identify the morphology and structure of the products. The function of the active carbon in the thermal evaporation is to serve as a reducing agent, so as to obtain Sn and Zn vapor sources [19].

After the growth of Zn_2SnO_4/ZnO HNS on Cr comb-shape interdigitating electrodes, we coated a thin layer of Pd onto the surface of Zn_2SnO_4/ZnO HNS by sputtering. The sputter current is 2 mA, and the deposition time is 300 s.

The heater of the gas sensor and the corresponding 3D schematic diagram are shown in Fig. 1c and d, respectively. The heater steel silks on the thermal insulation material are connected with the metal pins "1" and "4". Each gas sensor chip is put on the heater steel silks and bonded to another two metal pins so as to constitute sensor element as shown in Fig. 1e, and the corresponding 3D schematic diagram is show in Fig. 1f. When the heating voltage is applied to metal pins "1" and "4", the temperature of the heater steel silks will rise up according to Joule's law so as to make the temperature of gas sensor chip rise up. When the bias voltage is applied to metal pins "3" and "6", the electrical signal measurement for the gas sensor can be carried out. The sensor temperature at different heating voltage is measured by contacting a thermocouple to the upper side of gas sensor chip.

Each sensor element is packaged with a stainless steel mesh cap as shown in Fig. 1g. After that, the six metal pins of each sensor element are inserted the corresponding holes of one measurement unit in the test gas chamber as shown in Fig. 1h. There are ten measurement units in the test gas chamber, so 10 sensor elements can be tested at the same time. Then, the test gas chamber is sealed. By controlling gas-sensing characterization system (Gyjf Technology Co. Ltd., PR China/JFO2E) consisting of gas mixer instrument, measurement instrument and computer as show in Fig. 1i, certain concentration gas is passed into the test gas chamber based on a flow-through technique [20]. At the same time, >bias voltage of 8.9 V and certain heating voltage in the range of 3–6 V are supplied to test gas chamber so as to apply to each tested sensor element.

3. Results and discussions

The high magnified FESEM images of the comb-shape interdigitating Cr electrodes, the prepared Zn_2SnO_4/ZnO HNS distributing on the electrodes and the morphology of several Zn_2SnO_4/ZnO HNS are shown in Fig. 1j, k and l, respectively. The interspace between electrodes is 1.5 μm and the width of the electrode is 5 μm. In the Zn_2SnO_4/ZnO HNS, the width of the nanowires is about 20–30 nm, the side length and the thickness of the hexagon nanosheets are about 50 nm and 5 nm, respectively. Zn_2SnO_4/ZnO HNS overlap each other and form a networks structure, and such HNS networks provide large surface area in 3D space. Compared to the pressed nanograin thin film, in which only surface of the upper layer can be exposed to gas species, the HNS networks can, in principle, expose all the surface of each nanostructure to tested gas [21].

The morphology and structure of the as-synthesized Zn_2SnO_4/ZnO HNS samples are analyzed in detail by HRTEM in Fig. 2. The typical TEM bright-field images of some Zn_2SnO_4/ZnO HNS and an individual Zn_2SnO_4/ZnO HNS are shown in Fig. 2a and b, respectively. The corresponding EDS spectra in Fig. 2c show that the HNS in Fig. 2b is composed of O, Zn, Sn and Au. In addition, Cu and C are from the Cu net and C thin film in the process of TEM, respectively. The EDS elemental mappings in Fig. 2d–g show that element O and Zn distribute mainly in the nanosheet and slightly in the nanowire, element Sn distributes mainly in the nanowire, and element Au distributes mainly in the nanosheet as the catalyst according to the VLS mechanism in the process of nanostructures growth [22]. To be sure, in Fig. 2d–g, the *x*- and *y*-axes are added to accurately locate the position of the nanosheet so as to ascertain the existence area of every element in the HNS. Fig. 2h is a part and further magnified TEM bright-field image in Fig. 2b. In Fig. 2i, the HRTEM image recorded at the junction of nanowire and the nanosheet in the red frame in Fig. 2h shows that the interplanar spacing of 0.502 nm is corresponding to the (1 1 1) crystallographic plane of cubic Zn_2SnO_4 lattice, and the interplanar spacing of 0.248 nm is corresponding to the (1 0 1) crystallographic plane of hexagonal ZnO lattice. The corresponding fast Fourier transforms of the HRTEM image for Zn_2SnO_4, ZnO and the interface of Zn_2SnO_4/ZnO are shown in Fig. 2j, 2k and 2l, respectively. The fast Fourier transform in Fig. 2l comprises of two sets of patterns that are identified to be the cubic Zn_2SnO_4 structure (fast Fourier transforms in Fig. 2j) and hexagonal wurtzite ZnO structure (fast Fourier transforms in Fig. 2k), respectively. Above all, the nanowire is Zn_2SnO_4 and the nanosheet is ZnO in the HNS.

The morphology and structure of the Pd-Zn_2SnO_4/ZnO HNS are analyzed by HRTEM in Fig. 3. The whole Zn_2SnO_4/ZnO HNS is covered by numerous Pd nanoparticles with the size of 6–9 nm as shown in Fig. 3a. The corresponding EDS spectra in Fig. 3b show that the Pd-Zn_2SnO_4/ZnO HNS is composed of O, Zn, Sn, Au and Pd. The EDS elemental mappings in Fig. 3c–f show that the distributions of element O, Zn Sn and Au are same with those of the results in Fig. 2d–g, which is corresponding with the conclusions resulting from Fig. 2h–l that the nanowire is Zn_2SnO_4 and the nanosheet is ZnO in the Zn_2SnO_4/ZnO HNS. Besides, the EDS elemental mapping in Fig. 3g shows that element Pd distributes in the whole Zn_2SnO_4/ZnO HNS, which is corresponding with the image shown in Fig. 3a. The amount of deposited Pd nanoparticles in the Pd-Zn_2SnO_4/ZnO HNS is 1 wt%.

H_2 sensing characteristics are investigated when the sensors are exposed to different H_2 concentration of 2–1000 ppm, and operated at different heating voltage of 3 V, 4 V, 4.8 V, 5 V, and 6 V, corresponding to different substrate temperature of 120 °C, 200 °C, 255 °C, 270 °C, and 300 °C, respectively. The responses of the two kinds of sensors are shown in Fig. 4a and b, respectively. We calculated the response (relative resistance change) of the sensor using the expression of Response% = $(R_o - R_g)/R_o \times 100\%$ [23]. Here

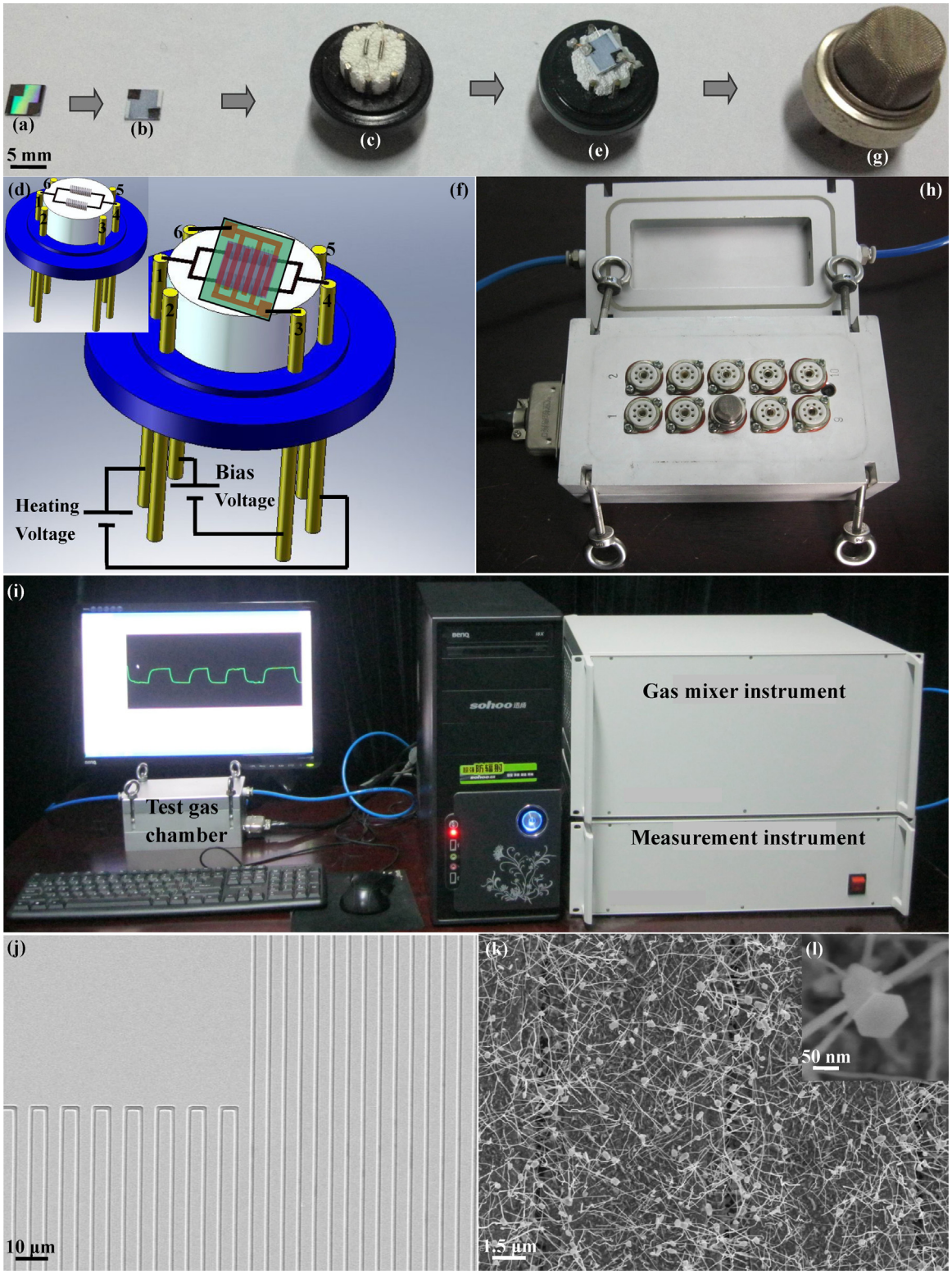

Fig. 1. The sensor element and gas-sensing characterization system: (a) comb-shape interdigitating Cr electrodes on the Si substrate; (b) Zn_2SnO_4/ZnO HNS gas sensor chip; (c) the heater of the gas sensor; (d) the 3D schematic diagram of the heater; (e) the sensor element; (f) the 3D schematic diagram of the sensor element; (g) sensor element packaged with a stainless steel mesh cap; (h) test gas chamber; (i) measurement instrument, gas mixer instrument and computer; the high magnified FESEM images of (j) the comb-shaped interdigitating Cr electrodes, (k) the prepared Zn_2SnO_4/ZnO HNS distributing on the electrodes and (l) the morphology of several Zn_2SnO_4/ZnO HNS.

R_o and R_g are the resistance of the sensor before and in exposing to the tested gas, respectively. The responses of the Zn_2SnO_4/ZnO HNS networks sensor are lower than those of Pd-Zn_2SnO_4/ZnO HNS networks sensor at every same concentration and same operating temperature. Fig. 4c and d shows the response as a function of operating temperature from 120 to 300 °C for two devices exposed to 2–1000 ppm H_2. Zn_2SnO_4/ZnO HNS networks sensor reaches the maximum response value of 46% at optimal operating temperature of 270 °C, while Pd-Zn_2SnO_4/ZnO HNS networks sensor reaches the maximum response value of 74% at optimal

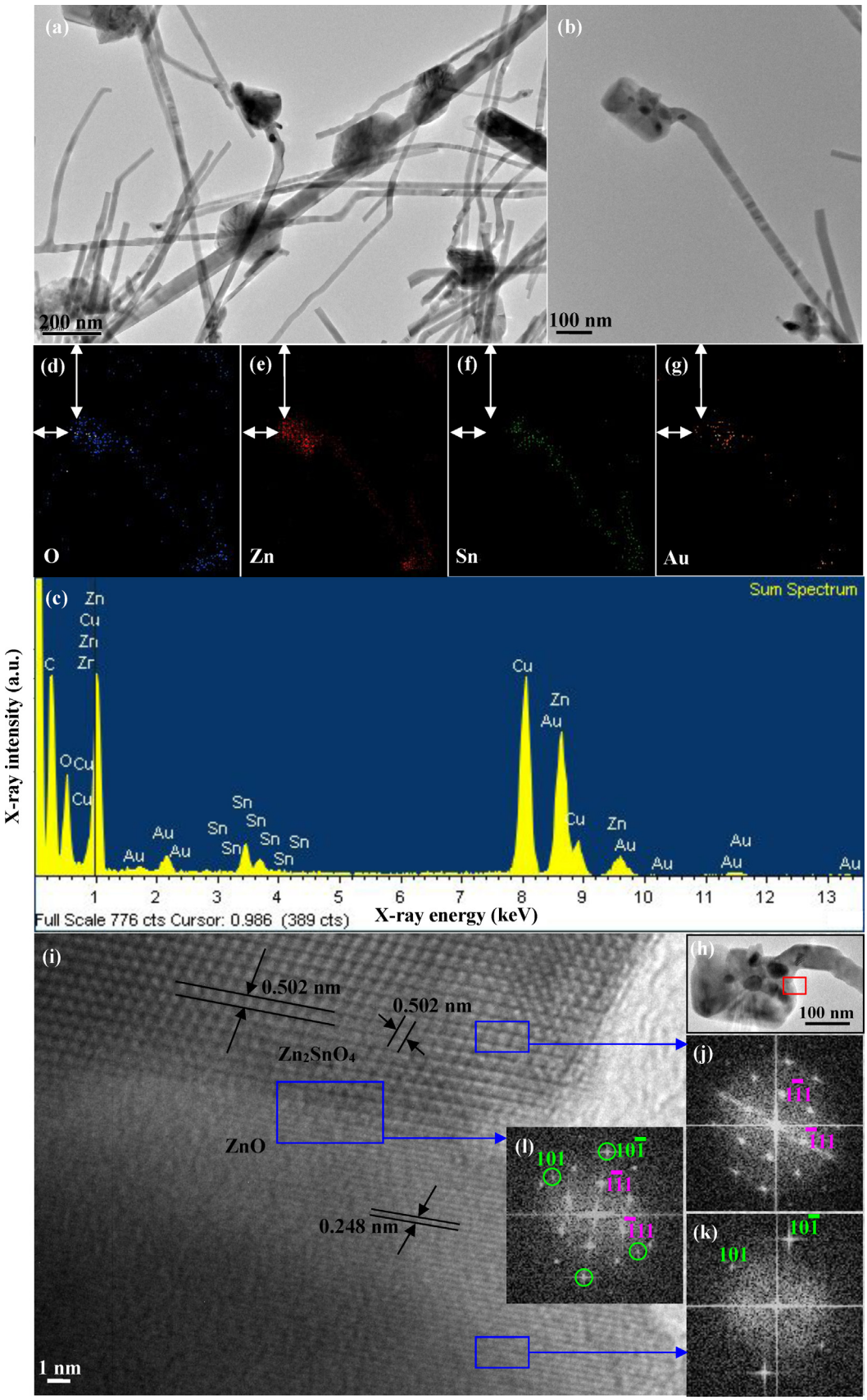

Fig. 2. The HRTEM characterized results of Zn_2SnO_4/ZnO HNS: >the >TEM bright-field images of (a) some Zn_2SnO_4/ZnO HNS and (b) an individual Zn_2SnO_4/ZnO HNS; (c) the EDS spectra, (d-g) the EDS elemental mappings, and (h) the part and further magnified TEM bright-field image of the single Zn_2SnO_4/ZnO HNS; (i) the HRTEM image of the interface of Zn_2SnO_4/ZnO; fast Fourier transforms of the HRTEM image for (j) the Zn_2SnO_4, (k) the ZnO and (l) the interface of Zn_2SnO_4/ZnO.

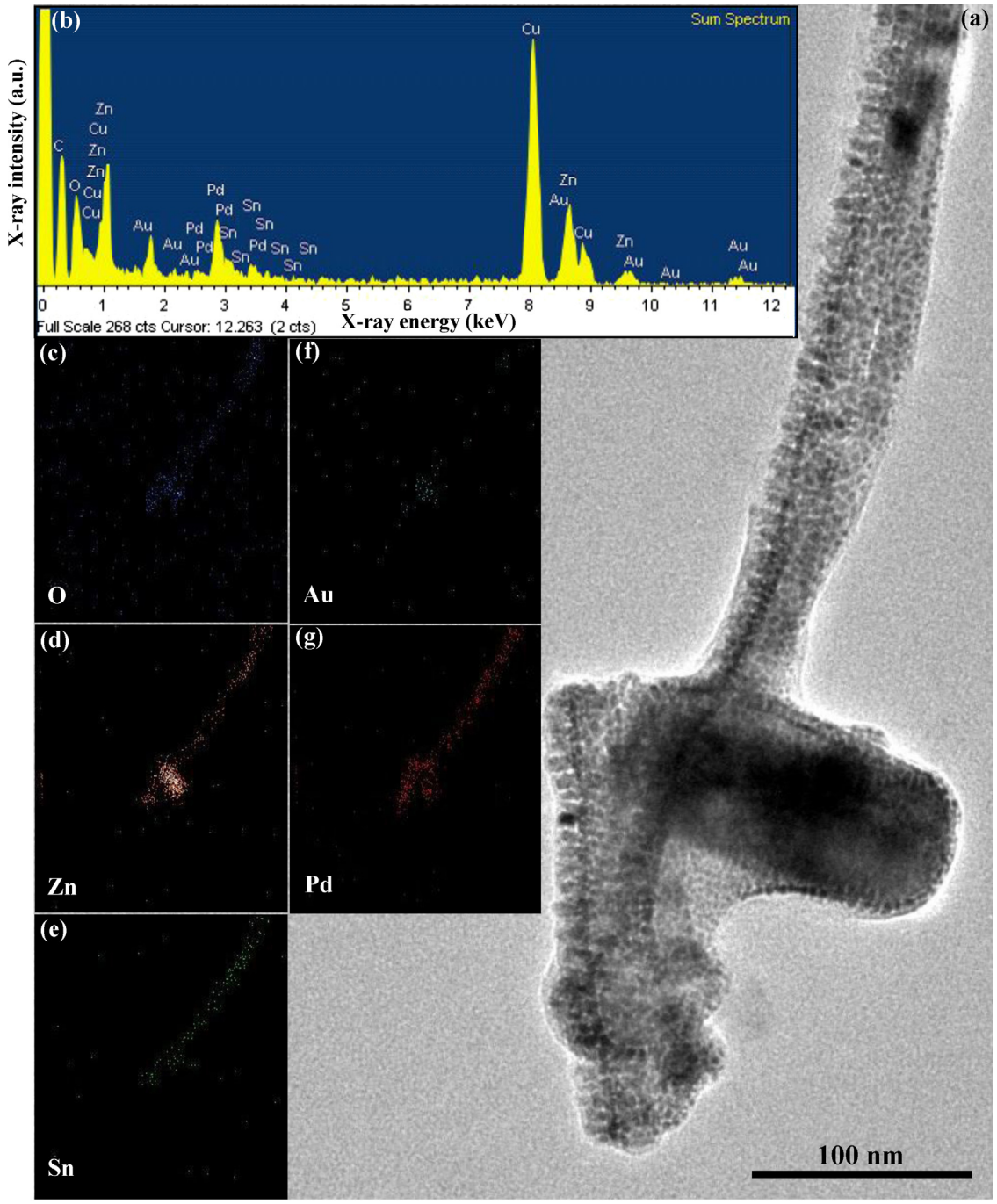

Fig. 3. The HRTEM characterized results of Pd-Zn_2SnO_4/ZnO HNS: >(a) the high magnified TEM bright-field image, (b) the EDS spectra, (c–g) the EDS elemental mappings of the Pd-Zn_2SnO_4/ZnO HNS.

operating temperature of 255 °C. By contrast, Pd-Zn_2SnO_4/ZnO HNS networks sensor results in higher response and lower optimal operating temperature to H_2.

The steady-state resistance response of the two kinds of sensors during exposure to increasing H_2 concentrations (between 2 and 1000 ppm) under respective optimal operating temperature of 255 °C or 270 °C is also investigated in Fig. 5a. According to the Zhu et al. [21], this should be done in a stable environment; and the time of measurement should be long enough to insure adsorption of hydrogen molecules to reach steady-state. Fig. 5b shows that the corresponding steady-state conductance ($G = 1/R$) of the two kinds of sensors follows a power law dependence on the H_2 gas concentration, $G_{gas} = G_{air} + \alpha(\text{concentration})^{\beta}$, where α is a constant, β is a power exponent [24]. By further derived based on the dynamic theory [25], $\alpha = e_0\mu\lambda(\xi/\eta)^{1/2}$. Where, the proportionality constant ξ is dimensionless and plays the role of a sticking or reaction coefficient; the proportionality constant η (cm^2/s) is the surface recombination coefficient which has an Arrhenius temperature dependence; λ is the sensor layer thickness, e_0 is the electronic charge magnitude, and μ is the electronic mobility. Variation of the microstructure can also change, sometimes dramatically, the relative values of α for different gases. Different α to variations in microstructure focuses attention on ways of obtaining controlled, reproducible, and regular microstructures with the critical dimensions commensurate with the Debye length of the oxide [26]. In addition, the β has some rational fraction value (usually 1 or

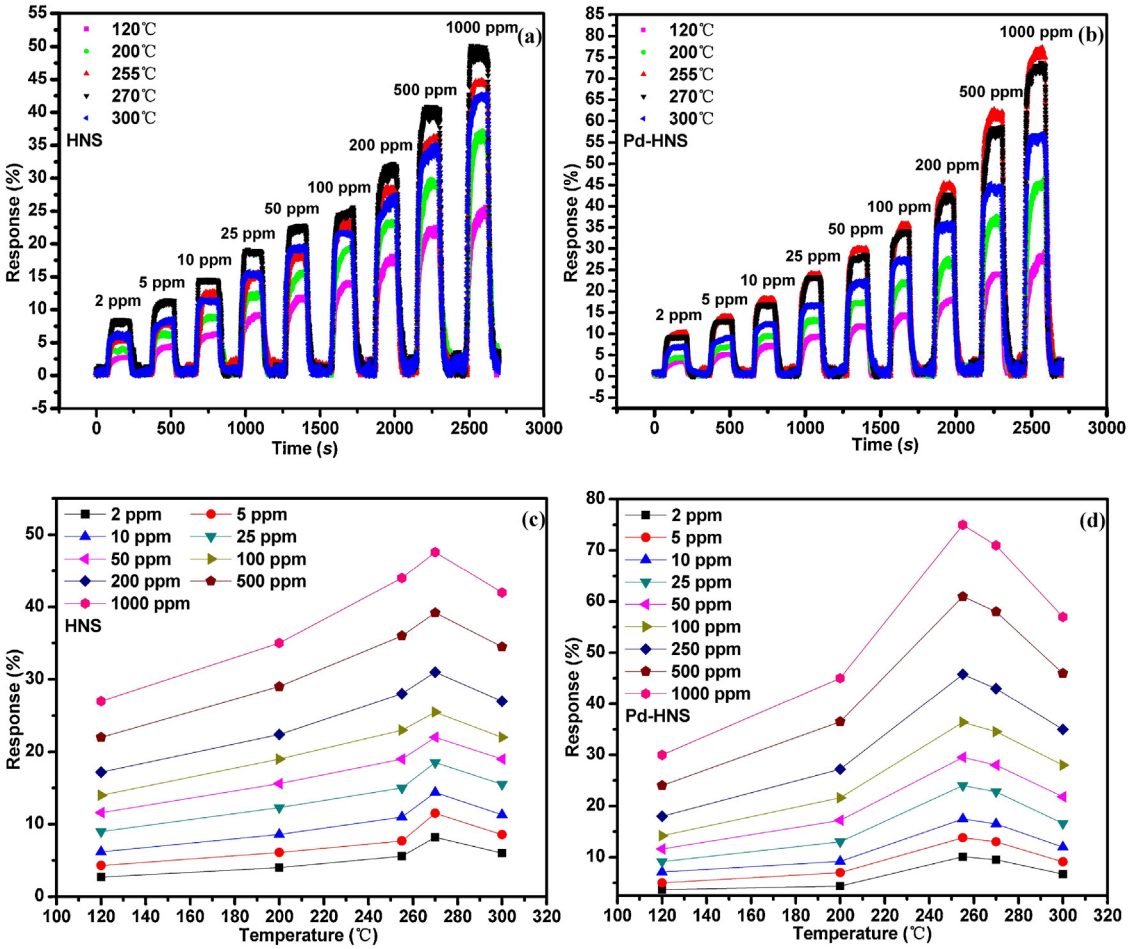

Fig. 4. Typical response curves of (a) Zn_2SnO_4/ZnO HNS networks sensor and (b) Pd-Zn_2SnO_4/ZnO HNS networks sensor exposed to H_2 concentrations ranging from 2 to 1000 ppm and tested at 120 °C, 200 °C, 255 °C, 270 °C, 300 °C, respectively; the response as a function of operating temperature of 120–300 °C exposed to 2–1000 ppm H_2 for (c) Zn_2SnO_4/ZnO HNS networks sensor and (d) Pd-Zn_2SnO_4/ZnO HNS networks sensor.

1/2), dependent on the charge of the surface species and the stoichiometry of the elementary reactions on the exterior. While the measurements often do give such rational values for the response exponent, non-rational values, different for different preparations of a given material in response to a given gas, are also frequently seen [26]. Studies of thin films imply that the response exponent for SnO_2, ZnO or Zn_2SnO_4, free of effects due to the microstructure, is $\beta = 0.5$ [25]. The expected response exponent for an "ideal" microstructure is $\beta = 0.5$ [24,26]. The effect of randomness in the microstructure is expected to be an increase of β above this value, and of agglomeration or of zones of the structure that are less gas sensitive than others is expected to be a decrease of β below this value [26]. The experimental data deduced from the measurement results in Fig. 5a are well consistent with the exponent fitting results, and the corresponding α, β, correlation coefficient R values obtained in the process of fitting are indicated in Fig. 5b. The somewhat difference between two α values of 1.22793×10^{-6} and 1.88408×10^{-6} is mainly due to different surface structures of two kinds of sensors [26]. For the β value of 0.39171 or 0.49623, the small deviations from the ideal value of 0.5 probably relate to either agglomeration or zones in the structure that are less sensitive to H_2 than others, as modeled recently by Scott et al. [26].

Response time is also an important parameter for a gas sensor, which are defined here as the time to reach 90% of the final equilibrium value [27]. The corresponding response times of the two kinds of sensors exposed to H_2 concentration of 2–1000 ppm at the operating temperature of 120 °C and 270 °C are indicated in Fig. 6a–d. The response times of the Zn_2SnO_4/ZnO HNS networks sensor are larger than those of the Pd-Zn_2SnO_4/ZnO HNS networks sensor at the same concentration and at the same operating temperature. The response time with respect to H_2 concentration of two kinds of sensors at the operating temperature of 120°C and 270 °C are shown in Fig. 6e and f, respectively. The reciprocal of the response time shows basically a linear relationship with H_2 concentration, and the reason is explained as follows. According to the Langmuir adsorption isotherm theory, in the case of the dissociation of a molecule into two species (H_2 into 2H), the process of adsorption is considered to be a reaction between the gas molecule and two surface sites [23]. At equilibrium (when the adsorption/desorption rates are equal), the relationship between the surface fraction occupied by adsorbates (Θ) and the pressure (P) or concentration of gas molecules is expressed as: $K_a \cdot P \cdot (1-\Theta)^2 = K_d \cdot \Theta^2$, or $\Theta/(1-\Theta) = (K \cdot P)^{1/2}$. Where the equilibrium constant (K) is defined by k_a/k_d, and k_a/k_d denote the adsorption/desorption rate constants, respectively. At the initial stage of the measurement, the rate of H_2 adsorption is $K_a \cdot P \cdot (1-\Theta)^2$, where $(1-\Theta)^2$ indicates the fraction of surface that is not covered by H_2. Since Θ is negligible at the initial stage, the adsorption rate is approximately $r \sim K_a \cdot P$. That is to say, initial H_2 adsorption rate follows a linear relationship with H_2 concentration. Moreover, the reciprocal of the response time is corresponding to the initial H_2 adsorption rate [23], so the reciprocal of the response time shows

Table 1
Hydrogen sensing characteristics of the Pd-Zn_2SnO_4/ZnO HNS networks sensor operated at 255 °C and Zn_2SnO_4/ZnO HNS networks sensor operated at 270 °C in comparison to those of the reported sensors using nanostructured materials.

Type	Operated temperature (°C)	Response ($\Delta R/R_o \times 100\%$) toward H_2 under the following concentrations (ppm)							Response time (s) to 150–270 ppm H_2
		2	10–50	50–270	400–500	1000	10,000	40,000	
Pd-Zn_2SnO_4/ZnO HNS	255	10	20	40	60	75	–	–	25
Zn_2SnO_4/ZnO HNS	270	8	15	28	38	47	–	–	29
Pt-$W_{18}O_{49}$ nanowires [21]	200	–	11.9	26.7	41.6	52.8	–	–	60
SnO_2 nanowire [30]	350	–	–	5	–	–	–	–	153
Pd-ZnO nanorods [28]	20–25	–	2.6	3.9	4.2	–	–	–	300–420
Pd-Ga nanowires [29]	20–25	–	–	7.4	8.3	8.6	–	–	300–420
Pt-SnO_2 nanowire [31]	200	–	–	–	–	–	50	–	<40
Single Pd nanowire [32]	20–25	–	–	–	–	–	–	8	120–600
ZnO nanorods [33]	20–25	–	4.2	5.5	7.6	–	–	–	600
ZnO/In_2O_3 nanorods [33]	20–25	–	9.8	15.5	20.5	–	–	–	400
Pt-InN nanowires [34]	20–25	–	2	3.1	–	–	–	–	300–420
Pt-GaN nanowires [35]	25	–	–	1.7	1.7	–	–	–	600
In_2O_3 nanowires [36]	200	–	–	17	60	–	–	–	31
In_2O_3 nanoneedles [36]	200	–	–	10.7	20	–	–	–	60
Pd-GaN nanowires [37]	25	–	–	12	13	14	–	–	30
Pd-InN nanobelts [37]	130	–	–	8	9	9.5	–	–	300
Pt-InN nanorods [37]	25	–	–	11	–	–	–	–	300
Pt-ZnO nanorods [37]	25	–	–	–	8	–	–	–	600
SnO_2/carbon nanotubes [38]	100	–	–	23	28.6	37.5	–	–	500

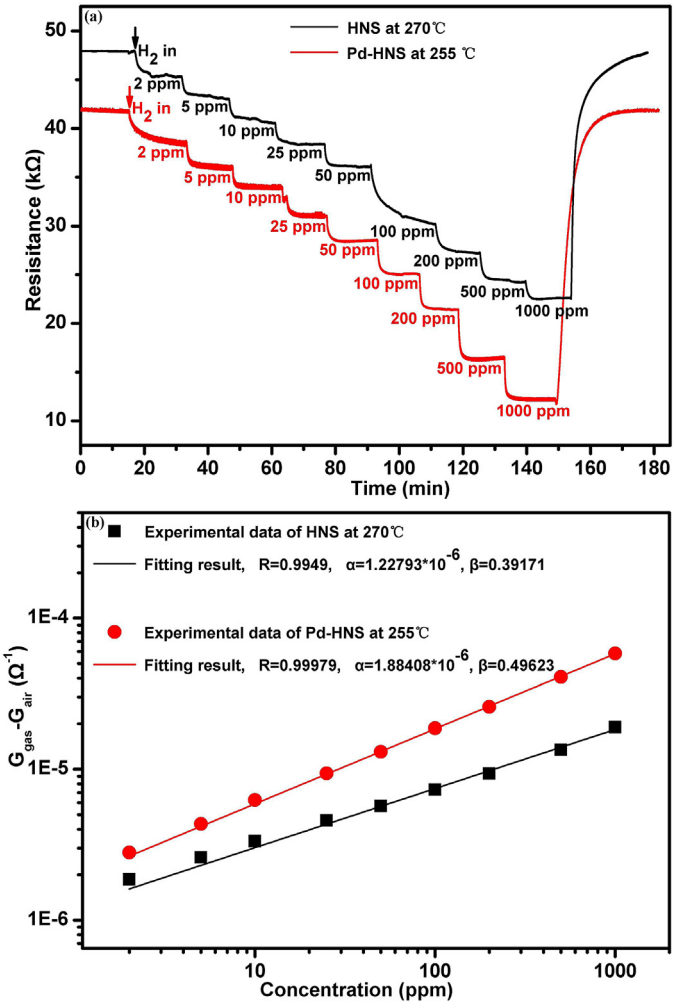

Fig. 5. (a) The steady-state resistance responses of two kinds of sensors during exposure to increasing H_2 concentrations (between 2 and 1000 ppm) under respective optimal operating temperature of 255 °C or 270 °C; (b) the corresponding steady-state conductance of both sensors as a function of the H_2 concentration.

basically a linear relationship with H_2 concentration as shown in Fig. 6e and f, which indicates that the sensing kinetics of the sensors mainly relied on the hydrogen dissociation process.

The time dependent of resistance of the Zn_2SnO_4/ZnO HNS networks and Pd-Zn_2SnO_4/ZnO HNS networks on exposure to 1000 ppm of H_2 at different operating temperature of 120–300 °C, are shown in Fig. 7a and b, respectively. The rate of resistance change becomes greater as temperature increases. The inset figures show the Arrhenius plot of rate of heterostructures resistance change. An adsorption activation energy of 14.98 kJ/mol for the Zn_2SnO_4/ZnO HNS networks as shown in Fig. 7a is larger than that of 12.72 kJ/mol for the Pd-Zn_2SnO_4/ZnO HNS networks as shown in Fig. 7b, that of 11.8 kJ/mol for the Pd-coated ZnO nanowires [28] and that of 2.2 kCal/mol for the Pd-coated GaN nanowires [29], but lower than that of 23.6 KJ/mol for the Pt-coated $W_{18}O_{49}$ nanowire networks [21].

The repeatability for H_2 (2 ppm, 10 ppm, 100 ppm, 1000 ppm) sensing at the operating temperature of 270 °C for the two kinds of sensors are shown in Fig. 8a and b, respectively. The response and recovery characteristics are repeatable when the sensing element is switched back and forth between air and H_2 gas environment.

Selectivity is one of the basic properties of gas sensor. The selectivity properties of the two kinds of sensors are tested within reducing gases such as CH_4, C_3H_8, C_2H_2, CO, C_2H_5OH, H_2, at the

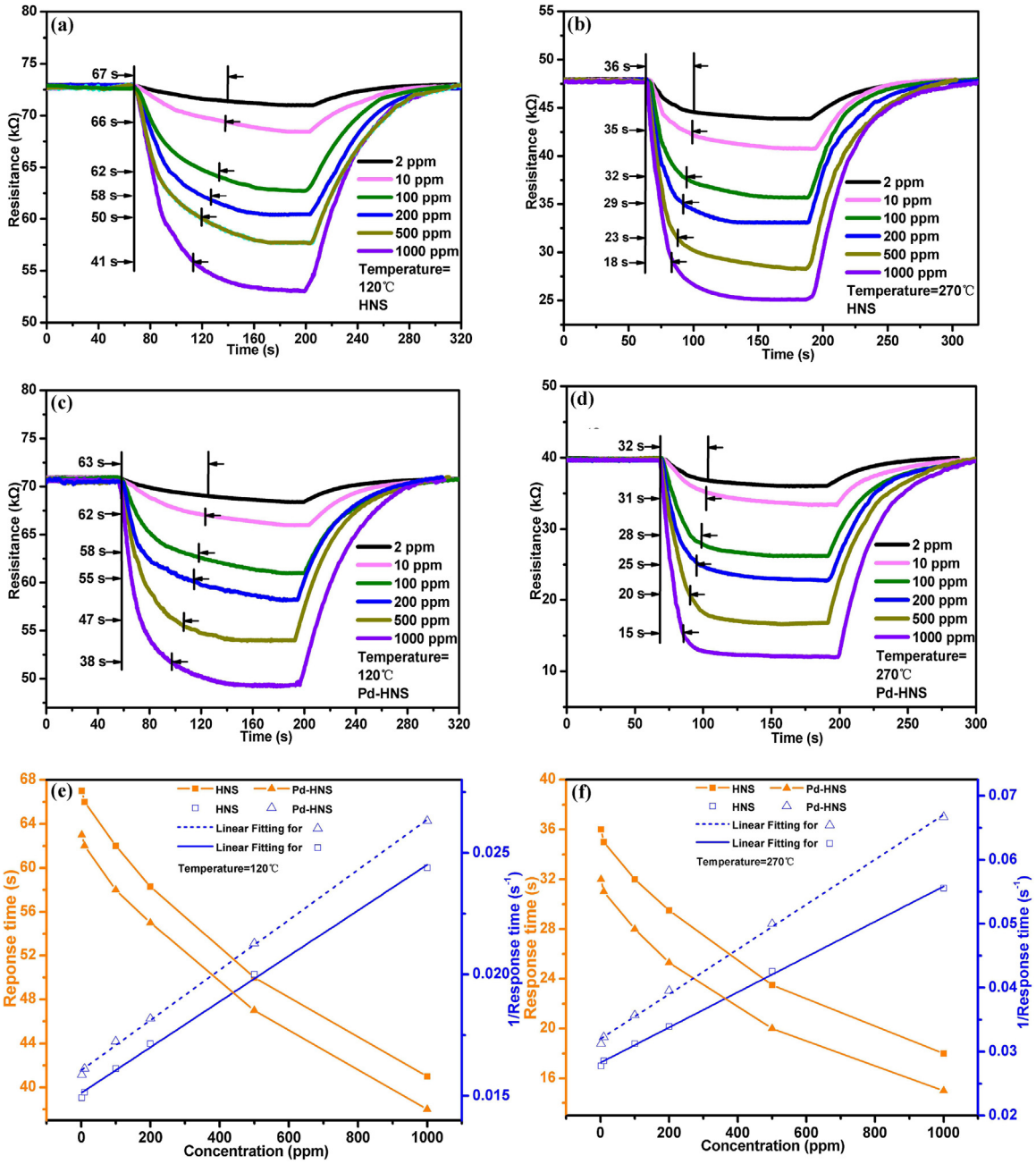

Fig. 6. One cycle of H_2 in and out in the concentration range of 2–1000 ppm under different operating temperature of 120 °C and 270 °C for (a), (b) Zn_2SnO_4/ZnO HNS networks sensor and (c), (d) Pd-Zn_2SnO_4/ZnO HNS networks sensor; the response time with respect to H_2 concentration of the two kinds of sensors at the different operating temperature of (e) 120 °C and (f) 270 °C.

concentration of 10 ppm, 100 ppm, 1000 ppm, under the different operating temperature of 120 °C (Fig. 9a) and 270 °C (Fig. 9b), respectively. It is very clear to discover that two kinds of sensors exhibit higher responses to H_2 in comparison with other gases, which indicates that both sensors have good selectivity properties. In addition, the responses of Pd-Zn_2SnO_4/ZnO HNS networks sensors to H_2 are higher than those of Zn_2SnO_4/ZnO HNS networks sensors at the same concentration and at the same operating temperature, so the selectivity of Pd-Zn_2SnO_4/ZnO HNS networks sensors to H_2 is better than that of Zn_2SnO_4/ZnO HNS networks sensors due to high H_2 solubility of Pd [15].

Considering the high operating temperature in the process of measurement possibly leading to the short life time, the long-term stability of the two kinds of sensors are also determined as shown in Fig. 10a and b, respectively. Clearly, the sensors show stable responses to 2–1000 ppm H_2 at operating temperature of 120–300 °C in 50 days, which confirms the high stability of the sensors at relatively high operating temperature.

H_2 sensing characteristics of the Pd-Zn_2SnO_4/ZnO HNS networks sensor operated at 255°C and Zn_2SnO_4/ZnO HNS networks sensor operated at 270°C in comparison to those of the reported sensors using nanostructured materials are shown in Table 1. The range of the responses of all the sensors normalized to $(R_o - R_g)/R_o \times 100\%$ is from 0% to 100% due to R_g smaller than R_o and greater than zero. Thus, these results definitely show that the self-assembly Zn_2SnO_4/ZnO HNS networks sensor and Pd-Zn_2SnO_4/ZnO HNS networks sensor have basically achieved better responses than those of the reported sensors [21,28–38]. In addition, the response times of the two kinds of sensors to 150–270 ppm H_2 are less than those of the reported sensors [21,28–38].

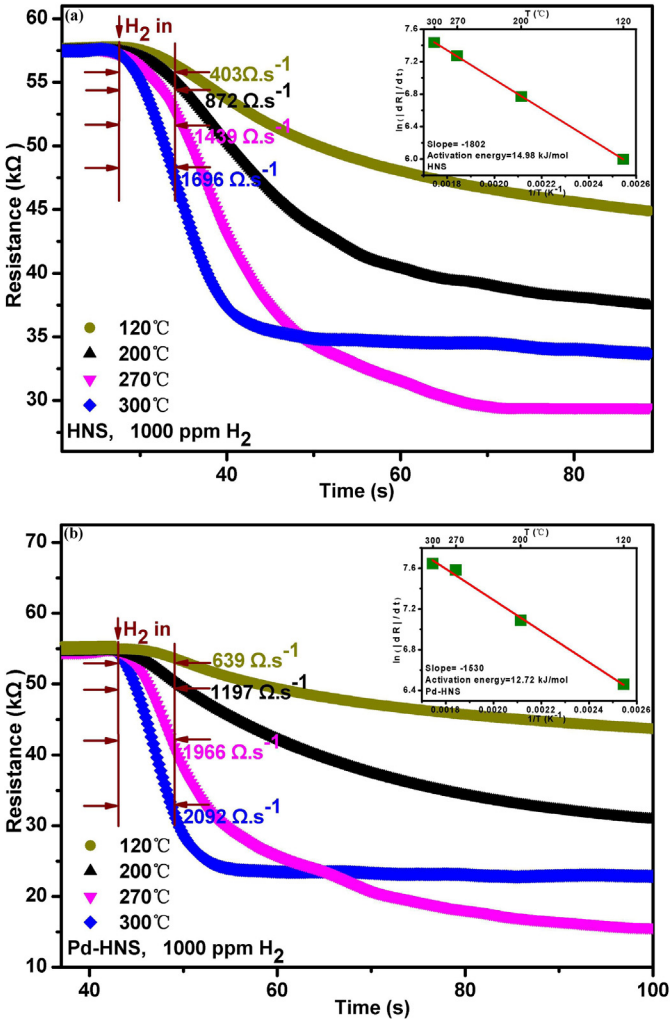

Fig. 7. Resistance vs. time on exposure to 1000 ppm of H_2 under different operating temperature of 120-300°C from (a) Zn_2SnO_4/ZnO HNS networks sensor and (b) Pd-Zn_2SnO_4/ZnO HNS networks sensor, the inset figures showing the corresponding Arrhenius plot based on the rates of change of the resistance.

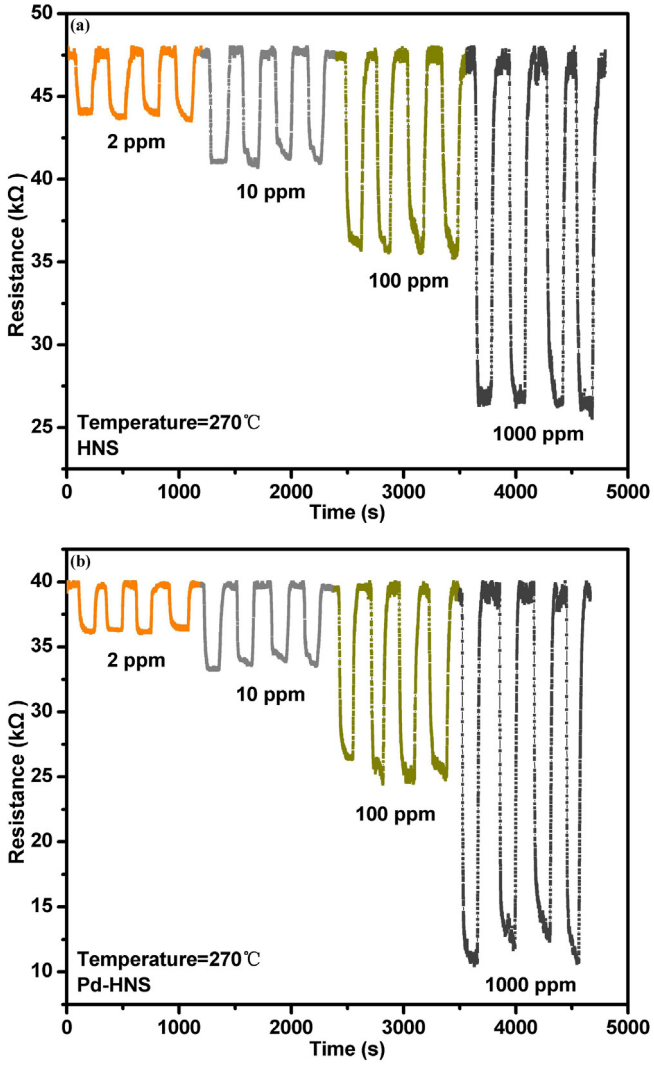

Fig. 8. Repeatability of the H_2 (2 ppm, 10 ppm, 100 ppm, 1000 ppm) sensing performance at the operating temperature of 270°C from (a) Zn_2SnO_4/ZnO HNS networks sensor and (b) Pd-Zn_2SnO_4/ZnO HNS networks sensor.

The H_2 sensing mechanism of Zn_2SnO_4/ZnO HNS investigated in this study is schematically described as follows. When the Zn_2SnO_4/ZnO HNS are exposed to air, the adsorbed oxygen molecules trapping electrons at the surface result in the presence of a depletion region in surface layer and narrow the conduction channels in the Zn_2SnO_4/ZnO HNS. In Zn_2SnO_4 nanowires or ZnO nanosheets, free carriers (electrons) can transport along the conduction channel. But when transporting between the overlapping Zn_2SnO_4/ZnO HNS, the electrons have to pass through potential barrier at the junctions and a thermoelectronic emission mechanism can be used to describe the electron transportation in the junctions [21]. In this paper, the overlapping Zn_2SnO_4/ZnO HNS affecting the electron transportation in the networked junctions can be summarized as three modes: the contact between two Zn_2SnO_4 nanowires, the contact between one Zn_2SnO_4 nanowire and one ZnO nanosheet, the contact between two ZnO nanosheets. The schematic illustration accounting for the three mechanisms operated in the networked HNS and the corresponding energy band diagram are shown in Fig. 11a. E_{vac}, E_c, E_v, and E_F are abbreviations of vacuum energy, conduction band minimum (CBM), valence band maximum (VBM), and Fermi level, respectively. Band gap of Zn_2SnO_4 and ZnO are 3.6 eV [39] and 3.37 eV [40], respectively. Work function of Zn_2SnO_4 and ZnO are 4.9 eV [41] and 5.0 eV [42], respectively. The change in resistance during the adsorption or desorption process of H_2 species is likely to be caused by the alteration both in the width of the surface depletion layer of each Zn_2SnO_4/ZnO HNS and in the height of potential barriers built at the networked junctions. These two-fold effects may facilitate less response time and higher response to certain chemical species [43].

The modulation of Zn_2SnO_4/ZnO HNS electrical transport properties through Pd nanoparticles is utilised to improve gas response. In the open air, the oxygen adsorbates (O_2^- or O^-) form on the surface of Pd [44], Zn_2SnO_4 [8] and ZnO [45] leading to a depletion region in surface layer owing to the electron shift from Pd, Zn_2SnO_4 and ZnO to oxygen. The sensing mechanism can be described as: H_2 reacts with oxygen adsorbates, which release electrons back to the surface of Pd-Zn_2SnO_4/ZnO HNS and alter its electrical conductivity of the structure [45]. The corresponding schematic illustration is shown in Fig. 11b. The enhanced sensing properties of the Pd-Zn_2SnO_4/ZnO HNS can be ascribed to an additional depletion layer at the interface between Pd nanoparticles and Zn_2SnO_4/ZnO HNS. The possible contribution is discussed as follows: The "electronic mechanism" proposes the formation of depletion zones around the particles and attributes the improved sensing to the modulation of the Schottky barrier [45]. Because the work function of Pd (5.12 eV) [44] is larger than that of Zn_2SnO_4 (4.9 eV) [41] and ZnO (5.0 eV) [42], the electrons in Zn_2SnO_4/ZnO

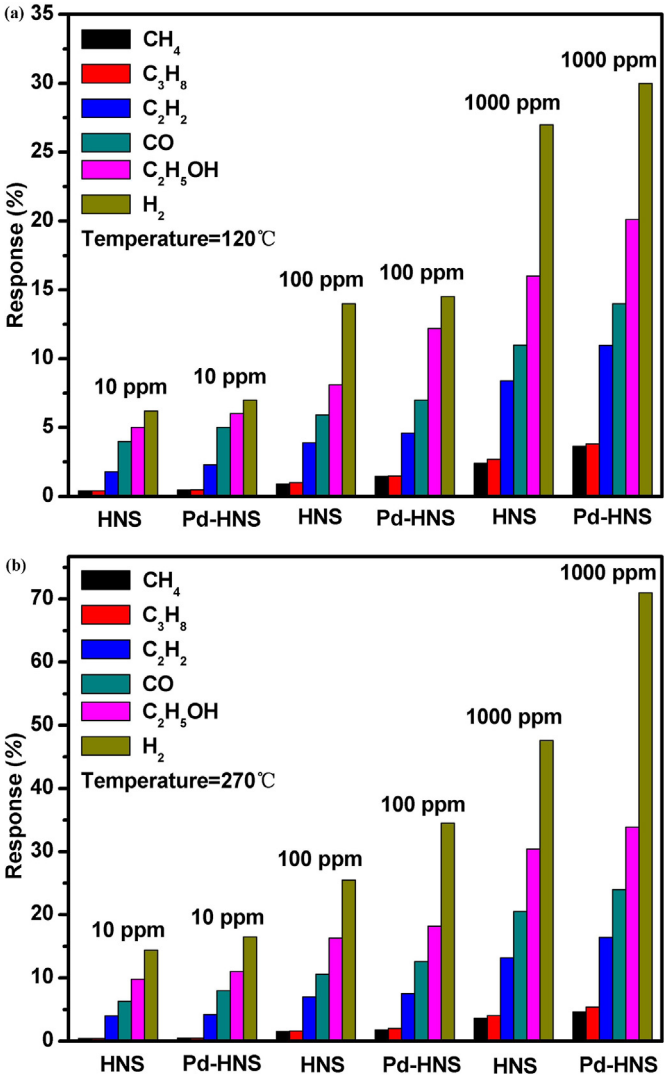

Fig. 9. The selectivity properties of two kinds of sensors to reducing gases such as CH_4, C_3H_8, C_2H_2, CO, C_2H_5OH, H_2, at the concentration of 10 ppm, 100 ppm, 1000 ppm, and under the different operating temperature of (a) 120 °C and (b) 270 °C.

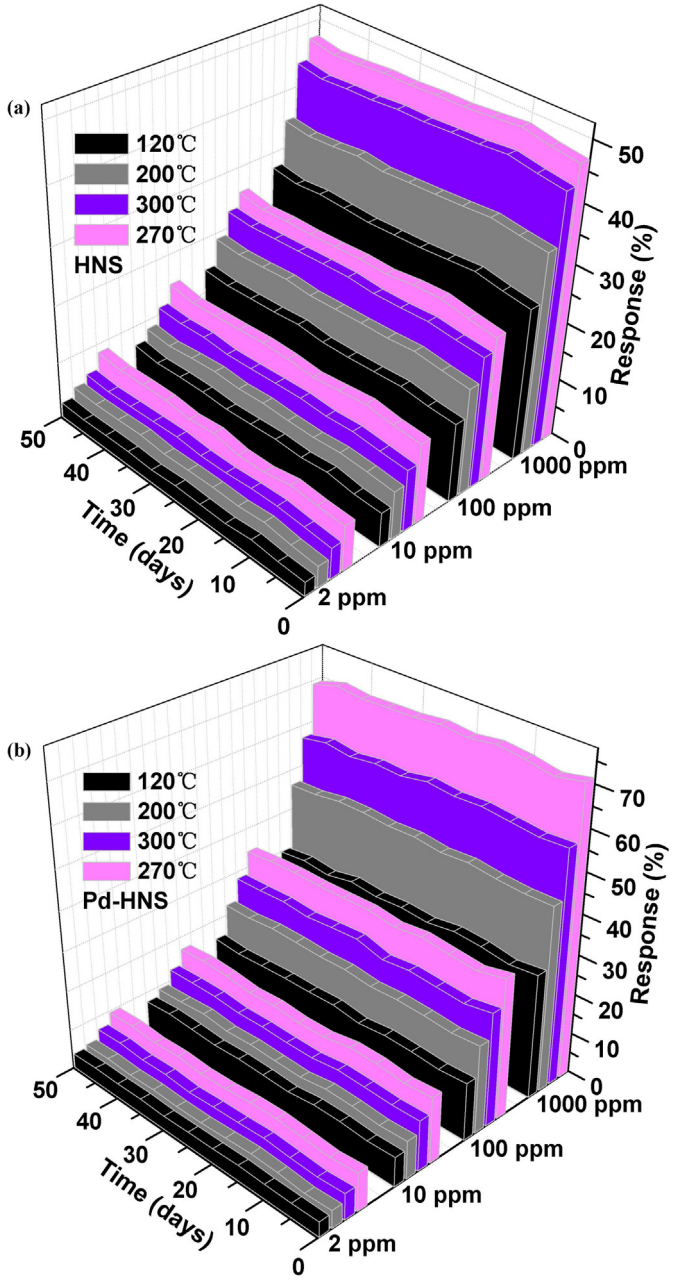

Fig. 10. Long-term stability to 2–1000 ppm H_2 at the operating temperature of 120–300 °C in 50 days for (a) Zn_2SnO_4/ZnO HNS networks sensor and (b) Pd-Zn_2SnO_4/ZnO HNS networks sensor.

HNS will transfer to Pd, thus leading to a Schottky barrier and an additional depletion layer at the interface. The conduction channel of Pd-Zn_2SnO_4/ZnO HNS is much narrower compared with Zn_2SnO_4/ZnO HNS. The electrons are released much easily from the surface reaction back into the conduction channel at the regions close to the Pd/Zn_2SnO_4 or Pd/ZnO interface, which greatly increases the conductivity of Pd-Zn_2SnO_4/ZnO HNS in H_2. Thus, these regions close to the Pd/Zn_2SnO_4 or Pd/ZnO interface make sensors more active in gas detection compared with that of the surface of bare Zn_2SnO_4/ZnO HNS. Meanwhile, additional the oxygen adsorbates (O_2^- or O^-) form on the surface of Pd nanoparticles onto Zn_2SnO_4/ZnO HNS by taking away electrons from Zn_2SnO_4/ZnO HNS [45]. Compared with bare Zn_2SnO_4/ZnO HNS, the attachment of Pd nanoparticles onto Zn_2SnO_4/ZnO HNS induces more active sites for the adsorption of oxygen molecules. Thus, these Pd regions on the surface of Zn_2SnO_4/ZnO HNS become high-performance gas sensing elements, making the sensors more active in H_2 detection than that of bare Zn_2SnO_4/ZnO HNS.

However, both sensors exhibit relatively low responses as compared to those reported in many previous works based on ZnO, and the reason can be possibly explained as follows: Firstly, the effective surface area is not as large as predicted because the porosity (voids) of the Zn_2SnO_4/ZnO HNS is high; Secondly, for the polycrystalline of Zn_2SnO_4/ZnO HNS networks containing Zn_2SnO_4 nanowire monocrystals and ZnO nanosheet monocrystals, the potential well can be formed in the ZnO nanosheets due to the barrier of the Zn_2SnO_4 nanowires being higher than that of the ZnO nanosheets, for the second and the third modes as shown in Fig. 11a. Therefore, the electrons are easily confined to the potential well of ZnO nanosheets between two barriers of the Zn_2SnO_4 nanowires so as to retard the electron transport through inter-grains, which can cause to a large resistance. Thirdly, for the first modes as shown in Fig. 11a, the relatively higher barrier of the Zn_2SnO_4 comparing with that of the ZnO may lead to the electron transportation in the junctions of bare ZnO being easier than that in the junctions of bare Zn_2SnO_4, which also brings about

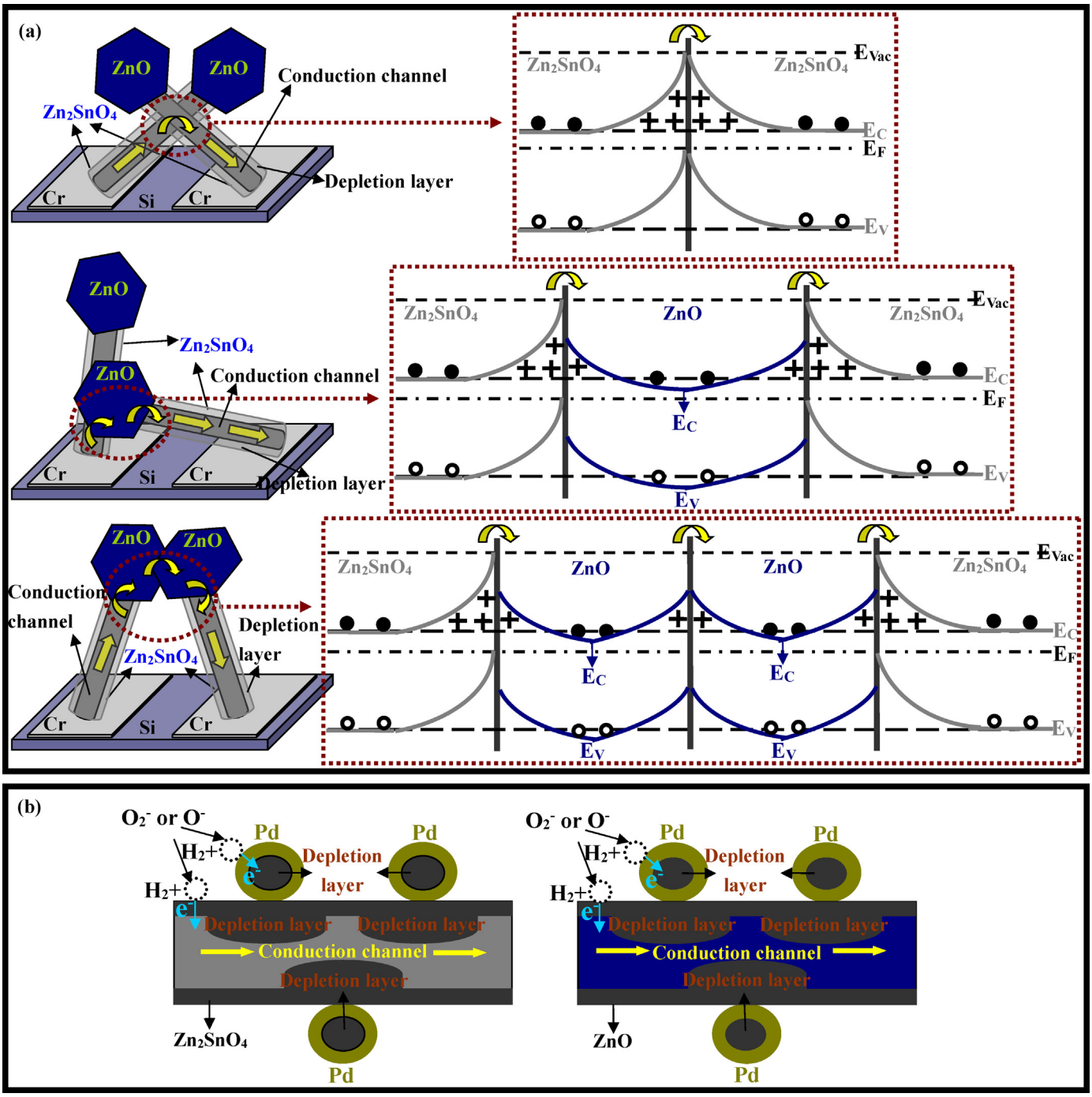

Fig. 11. (a) The schematic illustration accounting for the three mechanisms of the overlapping Zn_2SnO_4/ZnO HNS affecting the electron transportation operated in the networked HNS and the corresponding energy band diagram; (b) the schematic illustration accounting for the modulation of Zn_2SnO_4/ZnO HNS electrical transport properties through Pd nanoparticles for improving the gas response.

relatively low response of both sensors in comparison to those of many previously reported ZnO sensors.

4. Conclusions

In summary, we report that new Zn_2SnO_4/ZnO wire-sheet shape hetero-nanostructures have been synthesized via thermal evaporation and condensation with Au catalysts. The self-assembly sensors of Zn_2SnO_4/ZnO HNS networks on Cr comb-shape interdigitating electrodes with relatively narrower interspace of 1.5 μm have good selectivity, high response, low response time and adsorption activation energy, fine repeatability and long-term stability, small deviation from ideal value of power exponent β, in the hydrogen concentration range of 2–1000 ppm, and at the operating temperature of 120–300 °C. The alteration both in the width of surface depletion layer of each Zn_2SnO_4/ZnO HNS and in the height of potential barriers built at the networked junctions based on the three modes is attributed to the hydrogen sensing mechanism of Zn_2SnO_4/ZnO HNS networks during the adsorption or desorption process of H_2 species. In addition, the Pd decorated Zn_2SnO_4/ZnO HNS networks sensors exhibit an enhanced hydrogen sensing performance comparing with the Zn_2SnO_4/ZnO HNS networks sensors,

which is mainly resulting from an additional depletion layer at the interface between Pd nanoparticles and Zn_2SnO_4/ZnO HNS. For two kinds of sensors, the correlation between the response time and hydrogen concentration is in good agreement with the Langmuir adsorption isotherm model, which indicates that the sensing kinetics of the sensors mainly relied on the hydrogen dissociation process. Comparing with the Zn_2SnO_4/ZnO HNS networks sensors, the Pd decorated Zn_2SnO_4/ZnO HNS networks sensors could be more promising for further practical applications.

Acknowledgements

This work was supported by National Natural Science Foundation of China (50902097), Three Industry Basic Research Emphasis Project of Shenzhen (JC201104210013A), Guangdong Natural Science Foundation of China (9451806001002303), Outstanding young teacher training project in the institutions of higher learning of Guangdong Province, Open Project of Shenzhen Key Laboratory of Sensor Technology (SST201102), National Natural Science Foundation of China (51002192) and Project supported by the Foundation for the Author of Excellent Doctoral Dissertation of Guangdong Province.

This work is supported by Project of Department of Education of Guangdong Province (2013KJCX0165).

References

[1] J.X. Wang, X.W. Sun, S.S. Xie, Y. Yang, H.Y. Chen, G.Q. Lo, D.L. Kwong, Preferential growth of SnO_2 triangular nanoparticles on ZnO nanobelts, J. Phys. Chem. C 111 (2007) 7671–7675.
[2] R.C. Wang, J.S. Hung, ZnO-Sn:ZnO core–shell nanowires and ZnO-Zn_2SnO_4 comb-like nanocomposites, J. Nanosci. Nanotechnol. 10 (2010) 5634–5640.
[3] X.L. Bai, N. Pan, X.P. Wang, H.Q. Wang, Synthesis and photocatalytic activity of one-dimensional ZnO-Zn_2SnO_4 mixed oxide nanowires, Chin. J. Chem. Phys. 21 (2008) 81–86.
[4] J.X. Wang, X.W. Sun, Y. Yang, H. Huang, Y.C. Lee, O.K. Tan, L. Vayssieres, Hydrothermally grown oriented ZnO nanorod arrays for gas sensing applications, Nanotechnology 17 (2006) 4995–4998.
[5] J.Y. Park, D.E. Song, S.S. Kim, An approach to fabricating chemical sensors based on ZnO nanorod arrays, Nanotechnology 19 (2008), 105503 (5 pp.).
[6] Y. Zeng, T. Zhang, M.X. Yuan, M.H. Kang, G.Y. Lu, R. Wang, H.T. Fan, Y. He, H.B. Yang, Growth and selective acetone detection based on ZnO nanorod arrays, Sens. Actuators B 143 (2009) 93–98.
[7] J. Yi, J.M. Lee, W.I. Park, Vertically aligned ZnO nanorods and graphene hybrid architectures for high-sensitive flexible gas sensors, Sens. Actuators B 155 (2011) 264–269.
[8] J.H. Yu, G.M. Choi, Current–voltage characteristics and selective CO detection of Zn_2SnO_4 and ZnO/Zn_2SnO_4, SnO_2/Zn_2SnO_4 layered-type sensors, Sens. Actuators B 72 (2001) 141–148.
[9] H. Nanto, T. Morita, H. Habara, K. Kondo, Y. Douguchi, T. Minami, Doping effect of SnO_2 on gas sensing characteristics of sputtered ZnO thin film chemical sensor, Sens. Actuators B 35 (1996) 384–887.
[10] Y. Yamada, Y. Seno, Y. Masuoka, K. Yamashita, Nitrogen oxides sensing characteristics of Zn_2SnO_4 thin film, Sens. Actuators B 49 (1998) 248–252.
[11] G. Hu, H. Chen, Z.X. Chen, J.X. Zhang, H. Kohler, Humidity sensitive characteristics of Zn_2SnO_4–$LiZnVO_4$ thick films prepared by the sol–gel method, Sens. Actuators B 81 (2002) 308–312.
[12] S.T. Shishiyanu, T.S. Shishiyanu, O.I. Lupan, Sensing characteristics of tin-doped ZnO thin films as NO_2 gas sensor, Sens. Actuators B 107 (2005) 379–386.
[13] C.M. Chang, M.H. Hon, I.C. Leu, Improvement in CO sensing characteristics by decorating ZnO nanorod arrays with Pd nanoparticles and the related mechanisms, RSC Adv. 2 (2012) 2469–2475.
[14] Y. Zhang, Q. Xiang, J.Q. Xu, P.C. Xu, Q.G. Pan, F.J. Li, Self-assemblies of Pd nanoparticles on the surfaces of single crystal ZnO nanowires for chemical sensors with enhanced performances, J. Mater. Chem. 19 (2009) 4701–4706.
[15] C.M. Chang, M.H. Hon, I.C. Leu, Outstanding H_2 sensing performance of Pd nanoparticle-decorated ZnO nanorod arrays and the temperature-dependent sensing mechanisms, ACS Appl. Mater. Interfaces 5 (2013) 135–143.
[16] Y. Zhang, J.Q. Xu, P.C. Xu, Y.H. Zhu, X.D. Chen, W.J. Yu, Decoration of ZnO nanowires with Pt nanoparticles and their improved gas sensing and photocatalytic performance, Nanotechnology 21 (2010) 285501 (7 pp).
[17] X.H. Liu, J. Zhang, X.Z. Guo, S.H. Wu, S.R. Wang, Amino acid-assisted one-pot assembly of Au, Pt nanoparticles onto one-dimensional ZnO microrods, Nanoscale 2 (2010) 1178–1184.
[18] B. Wang, L.F. Zhu, Y.H. Yang, N.S. Xu, G.W. Yang, Fabrication of a SnO_2 nanowire gas sensor and sensor performance for hydrogen, J. Phys. Chem. C 112 (2008) 6643–6647.
[19] C. Pang, B. Yan, L. Liao, B. Liu, Z. Zheng, T. Wu, H.D. Sun, T. Yu, Synthesis, characterization and opto-electrical properties of ternary Zn2SnO4 nanowires, Nanotechnology 21 (2010) 465706 (4 pp).
[20] I.S. Hwang, S.J. Kim, J.K. Choi, J.J. Jung, D.J. Yoo, K.Y. Dong, B.K. Ju, J.H. Lee, Large-scale fabrication of highly sensitive SnO_2 nanowire network gas sensors by single step vapor phase growth, Sens. Actuators B 165 (2012) 97–103.
[21] L.F. Zhu, J.C. She, J.Y. Luo, S.Z. Deng, J. Chen, X.W. Ji, N.S. Xu, Self-heated hydrogen gas sensors based on Pt-coated $W_{18}O_{49}$ nanowire networks with high sensitivity, good selectivity and low power consumption, Sens. Actuators B 153 (2011) 354–360.
[22] B. Wang, X. Jin, Z.B. Ouyang, P. Xu, Photoluminescence and field emission of 1D ZnO nanorods fabricated by thermal evaporation, Appl. Phys. A 108 (2012) 195–200.
[23] M.G. Chung, D.H. Kim, D.K. Seo, T. Kim, H.U. Im, H.M. Lee, J.B. Yoo, S.H. Hong, T.J. Kang, Y.H. Kim, Flexible hydrogen sensors using graphene with palladium nanoparticle decoration, Sens. Actuators B 169 (2012) 387–392.
[24] I. Kim, A. Rothschild, T. Hyodo, H.L. Tuller, Microsphere templating as means of enhancing surface activity and gas sensitivity of $CaCu_3Ti_4O_{12}$ thin films, Nano Lett. 6 (2006) 193–198.
[25] H. Windischmann, P. Mask, A model for the operation of a thin-film SnO_x conductance-modulation carbon monoxide sensor, J. Electrochem. Soc. 126 (1979) 627–633.
[26] R.W.J. Scott, S.M. Yang, G. Chabanis, N. Coombs, D.E. Willams, G.A. Ozin, Tin dioxide opals and inverted opals: near-ideal microstructures for gas sensors, Adv. Mater. 13 (2001) 1468–1472.
[27] J. Li, H.Q. Fan, X.H. Jia, Multilayered ZnO nanosheets with 3D porous architectures: synthesis and gas sensing application, J. Phys. Chem. C 114 (2010) 14684–14691.
[28] H.T. Wang, B.S. Kang, F. Ren, L.C. Tien, P.W. Sadik, et al., Hydrogen-selective sensing at room temperature with ZnO nanorods, Appl. Phys. Lett. 86 (2005) 243503 (3 pp).
[29] W. Lim, J.S. Wright, B.P. Gila, J. Johnson, A. Ural, T. Anderson, F. Ren, S.J. Pearton, Room temperature hydrogen detection using Pd-coated GaN nanowires, Appl. Phys. Lett. 93 (2008) 072109 (3 pp).
[30] E. Bruneta, T. Maiera, G.C. Mutinati, S. Steinhauera, A. Köcka, C. Gspanb, W. Grogger, Comparison of the gas sensing performance of SnO_2 thin film and SnO_2 nanowire, Sens. Actuators B 165 (2012) 110–118.
[31] N.V. Duy, N.D. Hoa, N.V. Hieu, Effective hydrogen gas nanosensor based on bead-like nanowires of platinum-decorated tin oxide, Sens. Actuators B 173 (2012) 211–217.
[32] V.L. Ferrara, B. Alfano, G. Fiorentino, T. Polichetti, E. Massera, G.D. Francia, Nanopatterned platinum electrodes by focused ion beam in single palladium nanowire based devices, Microelectron. Eng. 88 (2011) 3261–3266.
[33] B.R. Huang, J.C. Lin, Core–shell structure of zinc oxide/indium oxide nanorod based hydrogen sensors, Sens. Actuators B 174 (2012) 389–393.
[34] W. Lim, J.S. Wright, B.P. Gila, S.J. Pearton, F. Ren, W.T. Lai, L.C. Chen, M.S. Hu, K.H. Chen, Selective-hydrogen sensing at room temperature with Pt-coated InN nanobelts, Appl. Phys. Lett. 93 (2008) 202109 (3 pp).
[35] J.S. Wright, W. Lim, B.P. Gila, S.J. Pearton, J.L. Johnson, A. Ural, F. Ren, Hydrogen sensing with Pt-functionalized GaN nanowires, Sens. Actuators B 140 (2009) 196–199.
[36] A. Qurashi, E.M. El-Maghrabyc, T. Yamazaki, T. Kikuta, Catalyst supported growth of In_2O_3 nanostructures and their hydrogen gas sensing properties, Sens. Actuators B 147 (2010) 48–54.
[37] J.S. Wright, W. Lim, D.P. Norton, S.J. Pearton, F. Ren, J.L. Johnson, A. Ural, nitride and oxide semiconductor nanostructured hydrogen gas sensors, Semicond. Sci. Technol. 25 (2010) 024002 (8 pp).
[38] M. Yang, D.H. Kim, W.S. Kim, T.J. Kang, B.Y. Lee, S. Hong, Y.H. Kim, S.H. Hong, H_2 sensing characteristics of SnO_2 coated single wall carbon nanotube network sensors, Nanotechnology 21 (2010) 215501 (7 pp).
[39] L.S. Wang, X.Z. Zhang, X. Liao, W.G. Yang, A simple method to synthesize single-crystalline Zn_2SnO_4 (ZTO) nanowires and their photoluminescence properties, Nanotechnology 16 (2005) 2928–2931.
[40] B. Wang, X. Jin, Z.B. Ouyang, P. Xu, Field emission properties originated from 2D electronics gas successively tunneling for 1D heterostructures of ZnO nanobelts decorated with In_2O_3 nanoteeth, J. Nanopart. Res. 14 (2012) 1008 (11 pp).
[41] C. Pang, B. Yan, L. Liao, B. Liu, Z. Zheng, T. Wu, H.D. Sun, T. Yu, Synthesis, characterization and opto-electrical propertiesof ternary Zn_2SnO_4 nanowires, Nanotechnology 21 (2010) 465706 (4 pp).
[42] S.L. Zhang, Y.H. Zhang, S.P. Huang, H. Liu, P. Wang, H.P. Tian, First-principles study of field emission properties of graphene-ZnO nanocomposite, J. Phys. Chem. C 114 (2010) 19284–19288.
[43] Y.K. Park, S.S. Kim, Formation of networked ZnO nanowires by vapor phase growth and their sensing properties with respect to CO, Mater. Lett. 65 (2011) 2755–2757.
[44] L.L. Xing, C.H. Ma, Z.H. Chen, Y.J. Chen, X.Y. Xue, High gas sensing performance of one-step-synthesized Pd–ZnO nanoflowers due to surface reactions and modifications, Nanotechnology. 22 (2011) 215501 (7 pp).
[45] J.L. Zhai, L.L. Wang, D.J. Wang, H.Y. Li, Y. Zhang, D.Q. He, T.F. Xie, Enhancement of gas sensing properties of CdS nanowire/ZnO nanosphere composite materials at room temperature by visible-light activation, ACS Appl. Mater. Inter. 3 (2011) 2253–2258.

Biographies

Bing Wang received her Ph.D. degrees in materials physics and chemistry from SunYat-sen University in China at 2007. In 2007, she joined Shenzhen University in China as a Lecturer and became a Associate Professor of Optoelectronic engineering at 2009. Her research interests include (i) development of new nanomaterials for the gas sensor applications, (ii) sensor devices, (iii) micro-fabrication process, (iv) vacuum micro/nanoelectronics, and (v) optical characteristics of nanomaterials.

Zhao Qiang Zheng received his B.E. degree from Hunan University in China at 2010. Currently, he is studying for M.Sc. degree at Shenzhen University in China. His research activities are focused on the surface physics and chemistry of metal oxides, development of new nanomaterials for the gas sensor applications and sensor devices.

Lian Feng Zhu received his Ph.D. degree in electronic materials from Sun Yat-sen University in China at 2011. Currently, he is working at Tsinghua University in China. His research activities are focused on the surface physics and chemistry of metal oxides, development of new nanomaterials for the gas sensor applications and sensor devices.

Yu Hua Yang received her Ph.D. degrees in materials physics and chemistry from Sun Yat-sen University in China at 2008. Since 2008, she has been working at Sun Yat-sen University. Her main research interests are ZnO-based nanomaterials and optical characteristics of nanomaterials.

Huan Yu Wu received his B.E. degree from Shenzhen University in China at 2010. Currently, he is studying for M.Sc. degree at Shenzhen University. His research activities are focused on vacuum micro/nanoelectronics, and optical characteristics of nanomaterials.